


Article

Electrochemical Deposition of Bismuth on Graphite Felt Electrodes: Influence on Negative Half-Cell Reactions in Vanadium Redox Flow Batteries

Shengbin Chen ^{1,†}, Chuanyu Sun ^{2,†} , Huan Zhang ^{1,*}, Hao Yu ¹ and Wentong Wang ¹¹ School of Textile and Material Engineering, Dalian Polytechnic University, Dalian 116034, China² School of Electrical Engineering and Automation, Harbin Institute of Technology, Harbin 150006, China; chuanyu.sun@mail.polimi.it

* Correspondence: zhanghuan_chndl@163.com

† These authors contributed equally to this work.

Abstract: In this paper, bismuth (Bi) was successfully deposited on graphite felts to improve the electrochemical performances of vanadium redox flow batteries. Modified graphite felts with different Bi particle loadings were obtained through electrochemical deposition at voltages of 0.8 V, 1.2 V and 1.6 V in 0.1 M BiCl₃ solution for 10 min. The optimal Bi particle loading was confirmed by scanning electron microscopy (SEM), single cells and electrochemical tests. The SEM images revealed the deposition of granular Bi particles on the fiber surface. The Bi-modified felts which were electrochemically deposited at 1.2 V (Bi/TGF-1.2V) showed excellent electrochemical performances in cyclic voltammetry curves and impedance spectroscopy. Meanwhile, the single cells assembled with Bi/TGF-1.2V as negative electrodes exhibited higher voltage efficiencies than the others. The optimized Bi particle loading induced better catalysis of the V³⁺/V²⁺ reaction and hence significantly improved the cell performances. In addition, the prepared Bi-modified felts showed stable cell performances and slower charge–discharge capacity declines than the other electrodes at current densities between 20 mA/cm² and 80 mA/cm². Compared with the pristine felt, the voltage efficiency of the vanadium redox flow battery assembled with Bi/TGF-1.2V graphite felt was 9.47% higher at the current density of 80 mA/cm². The proposed method has considerable potential and guiding significance for the future modification of graphite felt for redox flow batteries.

Keywords: vanadium redox flow battery; graphite felt; electro-chemical deposition; bismuth; electrochemical performance; cyclic voltammetry curve; impedance spectroscopy; capacity decay; voltage efficiency



Citation: Chen, S.; Sun, C.; Zhang, H.; Yu, H.; Wang, W. Electrochemical Deposition of Bismuth on Graphite Felt Electrodes: Influence on Negative Half-Cell Reactions in Vanadium Redox Flow Batteries. *Appl. Sci.* **2024**, *14*, 3316. <https://doi.org/10.3390/app14083316>

Academic Editors: Bogdan–Gabriel Burduhos, Gabriele Maria Lozito and Ahmed Elkafas

Received: 5 March 2024

Revised: 8 April 2024

Accepted: 9 April 2024

Published: 15 April 2024



Copyright: © 2024 by the authors. Licensee MDPI, Basel, Switzerland. This article is an open access article distributed under the terms and conditions of the Creative Commons Attribution (CC BY) license (<https://creativecommons.org/licenses/by/4.0/>).

1. Introduction

The continuous depletion of traditional fossil fuels and the resulting environmental problems have increasingly encouraged the development of renewable and green energy sources. However, renewable energy sources such as solar energy and wind energy are unstable and intermittent during generation, and thus these valuable electric energies are difficult to apply continuously and stably. To tackle this issue, the employment of large-scale energy storage systems combined with renewable energy may greatly improve the utilization rate and stability of renewable energy [1,2]. Redox flow batteries (RFBs) are considered to be one of the best choices for megawatt-level power storage, and megawatt demonstration systems have been installed, for example, in China, the United States, and Australia. RFBs are characterized by compact structures, long-life service, and can be charged quickly [3]. Hence, they are not only suitable for energy storage systems of wind power and photovoltaics but also can be used with the power grid. Compared with other energy storage batteries, vanadium redox flow batteries (VRFBs) have obvious advantages. The capacity and power of the battery can be adjusted flexibly according to the needs, and

the electrolyte is easy to recycle to restore the battery capacity and prolong the lifetime of the VRFB [4–6]. In particular, VRFBs have been widely studied as a new type of efficient, economical and environmentally friendly secondary batteries due to the wide standard reduction potentials of vanadium redox couples [7–9].

Key materials in VRFBs include electrodes, electrolytes, ion exchange membranes and current collector plates. The electrode does not participate in the redox reactions, only provides the reaction place, and electrons pass through the electrode/electrolyte interface to form a potential difference. After such a process, the VRFB can be charged and discharged based on the redox reactions of the vanadium redox couples. The electrolyte is composed of active substances and supporting electrolytes, in which the content of active substances determines the battery capacity, and supporting electrolytes can improve the conductivity of the electrolyte. The ion exchange membrane is used to separate positive and negative active substances, while selectively allowing the protons as the charge carriers to migrate through the membrane under the electric driving force to maintain electric neutrality and electrolyte balance.

The electrode materials play important roles in the performances of VRFBs because the redox reactions of vanadium ions occur on the electrode surface [10–12]. Graphite felt (GF) is used as the most common electrode material in VRFBs [13,14]. GF is characterized by a high specific surface area, strong oxidation resistance, corrosion resistance and high electrical conductivity. However, large-scale application of GF is limited by its poor hydrophilicity and electrochemical activity [15,16]. Tremendous efforts have been devoted to improving the electrochemical properties of GF. The modification of GF is mainly achieved by increasing the amount of active functional groups, enhancing the effective area, and introducing surface catalysts [17–19]. B. Sun et al. proposed that -OH and C=O functional groups are the main reasons for improving the electrochemical activity of carbon felt [20,21]. Since then, a large number of researchers have been dedicated to the preparation of hydrophilic GFs by heteroatom doping, such as N-doping [22] and B-doping [23,24]. Surface area is also the main reason affecting the electrochemical activity of carbon felt. Proper surface area means better diffusion and mass transfer of electrolytes on the surface of carbon felt [25–27]. The modification of GF with catalysts is a promising method to improve the electrochemical performances. Moreover, metal (In [28], Bi [29], Pb [30]), metal oxide (MnO [31], CoO [32], TiNb₂O₇ [33]) and activated carbon material (carbon nanotube [34], graphite oxide [35,36]) have been used to enhance the catalytic activity of GF.

In particular, bismuth is considered ‘the most cost-effective’ surface catalyst in VRFBs [37–40]. The methods employed for surface modification of GF by bismuth include in situ deposition and external deposition (e.g., hydrogen reduction, hydrothermal reaction) for VRFB applications [41–44]. However, in situ deposition is affected by many conditions, such as electrolyte flow rate, electrodeposition current density and initial concentration [41,45]. By contrast, external deposition is a better controllable method to modify GF with Bi. Recently, Zhang et al. introduced Bi on carbon felts by the electrooxidation processing in KOH and found that the VE of VRFB single-cells reached 73.4% at 400 mA/cm² [43]. Although bismuth has been successfully used in the electrode modification of VRFBs as a catalyst, the existing methods are not easy to apply due to extra hetero-ion introduction. To overcome the complex pretreatment procedures which are often employed during the modification of GF with Bi, electrochemical deposition was utilized to modify negative GF with Bi particles in this study. The proposed method was advantageous in terms of simple operation and short treatment periods. The GFs before and after modification with Bi were investigated by means of SEM, FTIR, XRD and electrochemical tests. In detail, the electrochemical tests refer to cyclic voltammetry (CV), linear sweep voltammetry (LSV), and electrochemical impedance spectroscopy (EIS). The catalytic effects of Bi particles on the electrochemical performances of VRFBs were also examined.

2. Experimental

2.1. Electrodes Modification

Polyacrylonitrile-based graphite felts (5 mm thickness, Gansu Haoshi Carbon Fiber Co., Ltd., Baiyin, China) were used as raw electrode materials. In order to achieve a higher carbon content, graphite felt generally needs to be treated at high temperatures to obtain a high graphitization degree. This also makes it have poor wettability, resulting in low electrochemical activity. Therefore, graphite felt must be activated properly before use. Such methods include heat treatment, surface deposition of catalysts, oxidation treatment, etc. [26,46]. Among them, the oxidation of graphite felt in hot air is considered to be the simplest and easiest method for industrialization. Therefore, based on previous work [13], the pristine graphite felts were pretreated by traditional thermal treatment at 500 °C for 5 h, and the obtained samples were denoted as TGF (thermally-treated graphite felt). Before the electrochemical deposition, TGF was washed with distilled water and dried at 80 °C for 24 h. The deposition process was carried out by using a constant voltage source (KXN-3010D, Shenzhen Zhaoxin Electronic Instrument Equipment Co., Ltd., Shenzhen, China) as the power source. The plating solution was prepared by dissolving a certain amount of Bi₂O₃ (99.0%, China National Pharmaceutical Chemical Reagent Co., Ltd., Shanghai, China) in the corresponding volume of dilute hydrochloric acid (3 M) to yield a 0.1 M Bi³⁺ solution. As shown in Figure 1, the TGFs (3.0 cm × 3.0 cm × 0.5 cm) were immersed in the solution as both the anode and the cathode. The distance between the anode and cathode was kept at approximately 3.0 cm. Copper wires were used to connect TGFs with the power source. After the TGFs were soaked in the 50 mL plating solution for 30 min, the metal Bi was reduced in the cathode side by the power source supplying a constant voltage for 10 min. The operating voltages were selected as 0.8 V, 1.2 V and 1.6 V, and the obtained samples were denoted as Bi/TGF-0.8V, Bi/TGF-1.2V and Bi/TGF-1.6V, collectively referred to as Bi/TGFs.

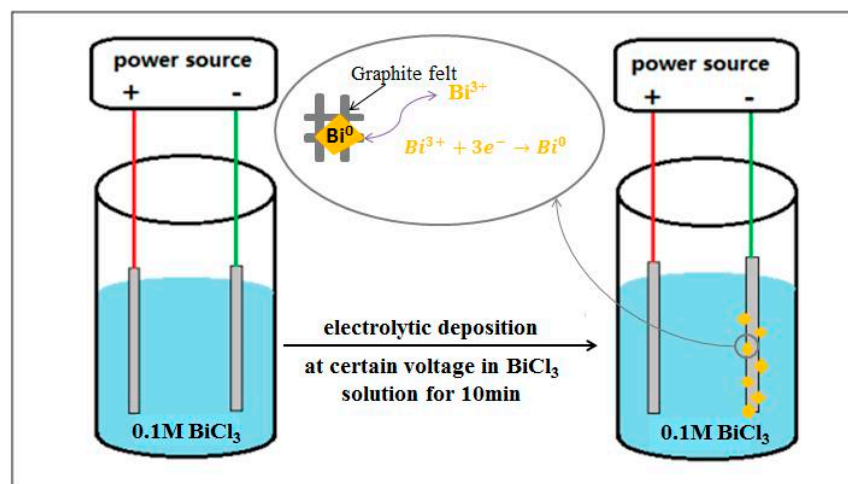


Figure 1. Schematic illustration of electrochemical deposition.

2.2. Characterization

A three-electrode system connected to an electrochemical workstation (CS310H CorrTest, Wuhan, China) was employed for electrochemical characterizations of the obtained electrodes at room temperature. The graphite felt with an area of 0.4 cm² was used as the working electrode, a 1 cm² platinum plate as the counter electrode, and a salt bridge filled with saturated potassium chloride solution as the reference electrode. The CV curves and EIS spectrogram were obtained in 1 M V³⁺ + 3.0 M H₂SO₄ electrolyte, and V³⁺ ions were obtained from electrolyzing the mixed solution of VOSO₄ (VOSO₄·xH₂O, >99%, x = 3.08, Shenyang Haizhongtian Fine Chemical Factory, Shenyang, China) and H₂SO₄ (98 wt.%, Guangzhou Donghong Chemical Factory, Guangzhou, China). CV measurements were

performed between 0 V and -0.8 V (vs. SCE) at a scan rate of 3 mV/s. The EIS spectrogram was obtained by applying a polarization potential of -0.4 V (vs. SCE) with 5 mV amplitude in the frequency range from 0.01 Hz to 100 kHz in the negative reaction. LSV curves were measured in 3 M H_2SO_4 and 1 M V^{3+} + 3 M H_2SO_4 solutions, respectively. The surface morphology of graphite felts before and after battery cycling tests was characterized by SEM (Nova Nano SEM 450AR Zeiss, Jena, Germany). The samples were tested by Nicolet iN10MX FT-IR analyzer and processed by the KBr tablet method. The scanning range was $400\text{--}4000\text{ cm}^{-1}$. The microcrystalline structure of the samples was measured by powder X-ray diffraction (XRD).

2.3. Cell Assembly and Test

The performances of electrode samples were tested in single dynamic cells. The 'TGF' before or after modification with Bi was used as the negative electrodes, and the 'TGF' was used as the positive electrodes. Both the negative and positive electrodes possess an active area of $3.0\text{ cm} \times 3.0\text{ cm}$. A perfluorinated ion-exchange membrane Nafion[®] 115 (DuPont, Wilmington, DE, USA) was employed to separate positive and negative electrolytes. Graphite plates were employed for charge collection and transfer. The above-mentioned three components were sealed with silicon rubber gaskets. The positive electrolyte was composed of 50 mL 1.0 M V^{4+} + 3.0 M H_2SO_4 , and the negative electrolyte was composed of 50 mL 1.0 M V^{3+} + 3.0 M H_2SO_4 . The electrolyte was stored in external tanks and cyclically pumped into the corresponding compartments during operation. The electrolyte flows through a peristaltic pump (MP-10R, Shanghai Zhiwo Pump Valve Co., Ltd., Shanghai, China) at a flow rate of 100 mL/min. The cells were monitored by a charge–discharge test system (CT2001C-5V/2A, Wuhan Land Co., Ltd., Wuhan, China) at the current density of 20–80 mA/cm² and the voltage window between 0.8 V and 1.65 V. The coulombic efficiency (CE), voltage efficiency (VE) and energy efficiency (EE) of single cells were estimated by the following formulas [47]:

$$\text{CE} = \frac{Q_{\text{discharge}}}{Q_{\text{charge}}} \times 100\% \quad (1)$$

$$\text{EE} = \frac{E_{\text{discharge}}}{E_{\text{charge}}} \times 100\% \quad (2)$$

$$\text{VE} = \frac{\text{EE}}{\text{CE}} \quad (3)$$

where Q_{charge} and $Q_{\text{discharge}}$ represent the charge and discharge capacity, respectively; E_{charge} and $E_{\text{discharge}}$ stand for the charge and discharge energy, respectively.

3. Results and Discussion

3.1. Electrochemical Performance

In Figure 2, the CV curves of TGF and Bi/TGFs are plotted in 1 M V^{3+} + 3 M H_2SO_4 solution. It can be seen that the curves of Bi/TGFs exhibit apparent current peaks, especially corresponding to the oxidation peak of $\text{V}^{2+} \rightarrow \text{V}^{3+}$. The oxidation peak currents of Bi/TGFs are 186 mA/cm² (Bi/TGF-0.8V), 218 mA/cm² (Bi/TGF-1.2V) and 207 mA/cm² (Bi/TGF-1.6V), respectively. The minimum oxidation peak is observed on the TGF (56 mA/cm²). Meanwhile, the TGF has the lowest electric double layer capacity (EDLC) of 4.085 F/cm². However, the EDLC values of Bi/TGFs are increased to 9.262 F/cm² (Bi/TGF-0.8V), 12.502 F/cm² (Bi/TGF-1.2V) and 11.480 F/cm² (Bi/TGF-1.6V), respectively. These results indicate that the Bi deposition on TGFs promotes the negative reaction of vanadium ions. In a comparison of the peak current and capacitance values, Bi/TGF-1.2V shows better electro-catalytic activity than the other samples.

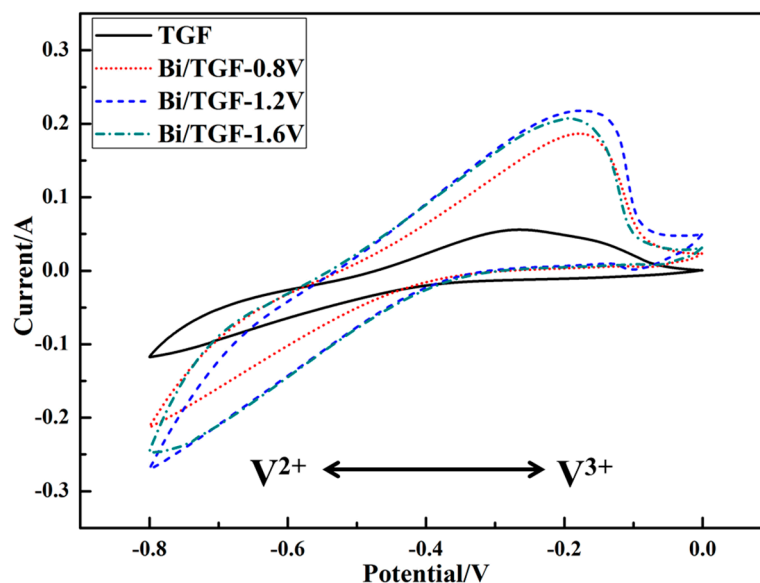


Figure 2. CV curves recorded in 1 M V^{3+} + 3 M H_2SO_4 solution at a scan rate of 3 mV/s.

Figure 3 shows the EIS spectrograms of samples in 1 M V^{3+} + 3 M H_2SO_4 solution at a polarization potential of -0.4 V (vs. SCE). The EIS spectrograms provide further analysis concerning the influence of Bi on the electrochemical properties of TGFs on the negative side. As shown in Figure 3, each EIS spectrogram includes a semicircle and a linear part. The semicircle at high frequencies (100 Hz to 100 kHz) reflects the charge transfer resistance, while the linear part at low frequencies (0.01 Hz to 100 Hz) is related to the diffusion of vanadium ions through the solution. Thus, the EIS spectrograms indicate that negative V^{3+}/V^{2+} redox couples on samples were mix-controlled by charge transfer and diffusion steps. The EIS spectrograms are fitted by an equivalent circuit in Figure 3, where R_s represents the bulk solution resistance, R_p stands for the charge transfer resistance of the electrochemical reactions, CPE is the constant phase element that accounts for double-layer capacitance, and W is Warburg impedance. The fitting results for all samples are given in Table 1. Although the pristine graphite felt had been pre-treated by the thermal method, the R_p of TGF for the V^{3+}/V^{2+} redox reaction was the largest, resulting in poor electrochemical activity. However, the R_p values of Bi/TGFs were smaller, suggesting that Bi is more effective in catalyzing negative electrode reactions. In Table 1, the R_p for Bi/TGF-0.8V, Bi/TGF-1.2V, and Bi/TGF-1.6V are $1.24 \Omega \cdot cm^2$, $0.89 \Omega \cdot cm^2$, and $1.39 \Omega \cdot cm^2$, respectively. The results indicate that the electrodeposition potential of 1.2 V can enhance the electron transfer rate of the V^{3+}/V^{2+} redox reaction.

Table 1. The parameters obtained from fitting EIS plots with the equivalent circuit.

Samples	R_s ($\Omega \cdot cm^2$)	CPE (T) ($\times 10^{-5}$)	CPE (P)	R_p ($\Omega \cdot cm^2$)	W (R)	W (T)	W (P)
TGF	0.68	8.49	1.11	1.69	2.48	0.002	0.365
Bi/TGF-0.8V	0.66	1.41	1.08	1.24	17.72	0.040	0.652
Bi/TGF-1.2V	0.64	1.13	1.11	0.89	1.50	0.001	0.384
Bi/TGF-1.6V	0.69	7.38	1.12	1.39	17.94	0.240	0.624

To deeply analyze the electrocatalytic mechanism of Bi toward the V^{3+}/V^{2+} redox couples, LSV is conducted for samples in 3 M H_2SO_4 and 1 M V^{3+} + 3 M H_2SO_4 , as shown in Figure 4. The potential reactions have been proposed in the literature [48]. The chemical equations are shown as follows:

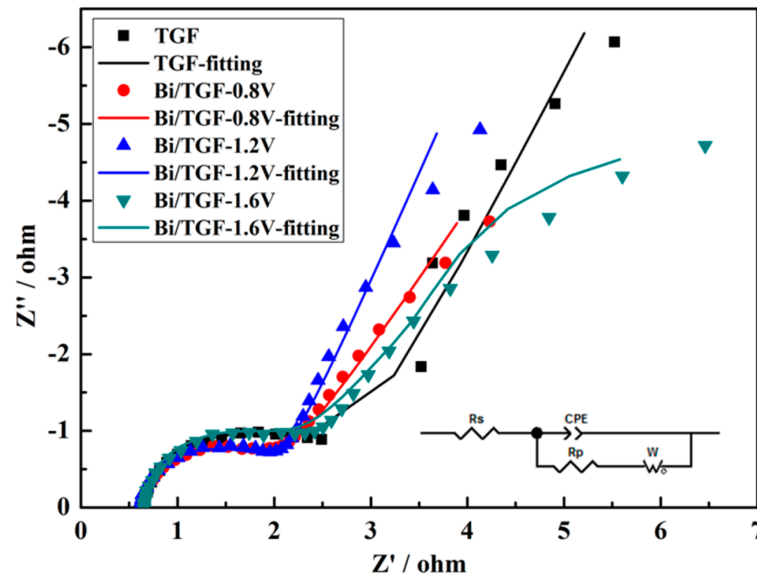
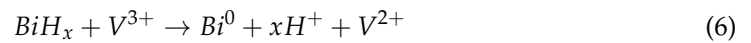


Figure 3. The EIS spectrograms recorded in 1 M V^{3+} + 3 M H_2SO_4 solution at DC voltage -0.4 V vs. SCE.

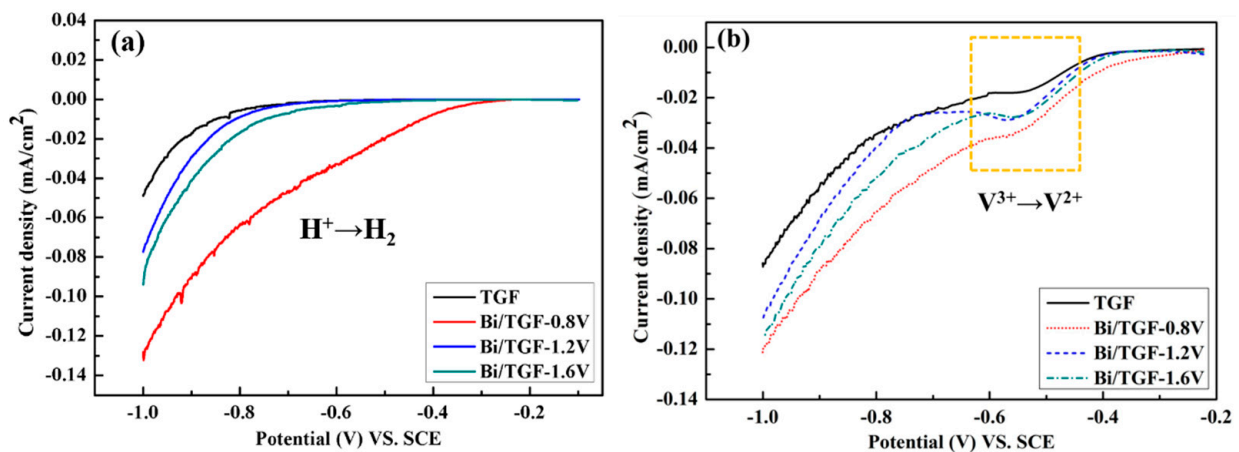


Figure 4. LSVs performed in (a) 3 M H_2SO_4 and (b) 1 M V^{3+} + 3 M H_2SO_4 solution at a scan rate of 1 mV/s.

The hydrogen evolution reaction (HER) is an unavoidable side reaction. Excessive hydrogen evolution will not only cause irreversible attenuation of cell capacity but also bring serious safety risks. Therefore, HER is a serious problem that must be explored in acidic electrochemical power sources. As shown in Figure 4a, the onset potential of the HER for TGF is the highest, which is found to be -0.72 V (vs. SCE) in the H_2SO_4 solution. The HER onset potentials of the Bi/TGFs shifted to a more positive position probably due to some additional reactions. Although bismuth has been known to inhibit HER ineffectively [30,43], the onset potentials of Bi/TGF-1.6V and Bi/TGF-1.2V are indeed much closer to the TGF. The electrodeposited Bi on the graphite felt is oxidized to form

BiH_x by combining with H^+ ions in the electrolyte. Therefore, the abrupt potential from the reduction curves of Bi/TGFs is assumed to be the reactions (5). The ability for the absorption of H^+ ion is in the order of $\text{TGF} < \text{Bi/TGF-1.2V} < \text{Bi/TGF-1.6V} < \text{Bi/TGF-0.8V}$ by decreasing current density [49]. The nonlinear relationship between the reaction activities of each sample to reactions (4,5) and the deposition voltage should be attributed to the morphology of Bi particles [43], which was further analyzed by the SEM results. As an intermediate product, BiH_x acts as an effective catalyst for the $\text{V}^{3+}/\text{V}^{2+}$ reaction, which makes the charge transfer of the reduction reaction faster in the reaction (6). As shown in Figure 4b, the reduction peak in $1 \text{ M V}^{3+} + 3 \text{ M H}_2\text{SO}_4$ is more pronounced. It is verified that the $\text{V}^{3+}/\text{V}^{2+}$ reduction potential is around -0.55 V (vs. SCE). The values of reduction current and reduction potential corresponding to Bi/TGFs are significantly higher than those of TGF. Considering the HER, the electrocatalytic performance of Bi/TGF-1.6V and Bi/TGF-1.2V for the $\text{V}^{3+}/\text{V}^{2+}$ redox couple is better than that of Bi/TGF-0.8V.

3.2. SEM, FTIR and XRD

To gain a better understanding of the relationship between the surface morphology and catalytic effect, the electrodes were subjected to SEM. Figure 5a–d depict the morphology of modified fibers surfaces with and without Bi particles at the same magnification. The surface of GF appeared to be clean and smooth as shown in Figure 5a, but the surface of Bi/TGFs was attached with Bi and the size of Bi increased with the increase in electrochemical deposition voltage. The bismuth of Bi/TGF-0.8V (Figure 5b) is in the grooves on the surface of the fibers, and bismuth of Bi/TGF-1.2V and Bi/TGF-1.6V attached to the surface of the fiber is crystallized into sheets in Figure 5c,d. According to the results of LSV, the HER and hydrogen ion absorption are preferentially carried out on the tiny Bi particles, as shown in Bi/TGF-0.8V. Therefore, too many flaky Bi particles, as shown in Bi/TGF-1.2V and Bi/TGF-1.6V, are not sensitive to HER and hydrogen ion absorption. Because of this, only an appropriate Bi loading can better catalyze the negative electrode reaction. This is the reason that the results of CV and EIS for Bi/TGF-1.2V are superior to that for Bi/TGF-1.6V. The XRD result of Bi/TGF-1.2V was reported in Figure 5e, which has a perfect match with the Pure Bi standard card, indicating that the metal Bi affects the catalyst on the surface of carbon fiber. And the comparison of FTIR results between GF and Bi/TGF-1.2V in Figure 5f showed that more oxygen-containing groups appeared on the GF surface after Bi deposition (-O-H stretching vibration peak: c.a. $3600\text{--}3200 \text{ cm}^{-1}$; alkyl C-H bending vibration peak: c.a. $2920\text{--}2850 \text{ cm}^{-1}$; -C=O stretching vibration peak: c.a. $1720\text{--}1750 \text{ cm}^{-1}$) [50]. It can be seen that the more active metal bismuth becomes the active center, so that the hydrophobic GF can absorb oxygen in the air and become a hydrophilic electrode material. To confirm the effect of Bi on enhanced electrochemical performances, the morphology of TGF acquired after 20 charge–discharge cycles in the cell was obtained, and the results are depicted in Figure 5g,h. The size of metal bismuth particles deposited on the surface of GF has always been a focus of researchers [42]. If only the catalytic activity of Bi is considered, then the nanoscale Bi will obviously be more active. However, the flow erosion of electrolytes and the electrolytic effect during the charge and discharge process will inevitably affect the existence of metal bismuth particles on the electrode surface and in the flow cells. This work attempts to control the deposition size and amount of Bi by electrodeposition voltage so that it can adapt to the internal environment of the VRFBs. Too large or too small scale of Bi is not conducive to its catalytic effect, so Bi/TGF-1.2V can be concluded to own the highest catalytic activity. EDS results showed that the Bi particles and electrolytes still remained on the surface of Bi/TGF-1.2V after 20 charge–discharge cycles (see it in the Supplementary Material).

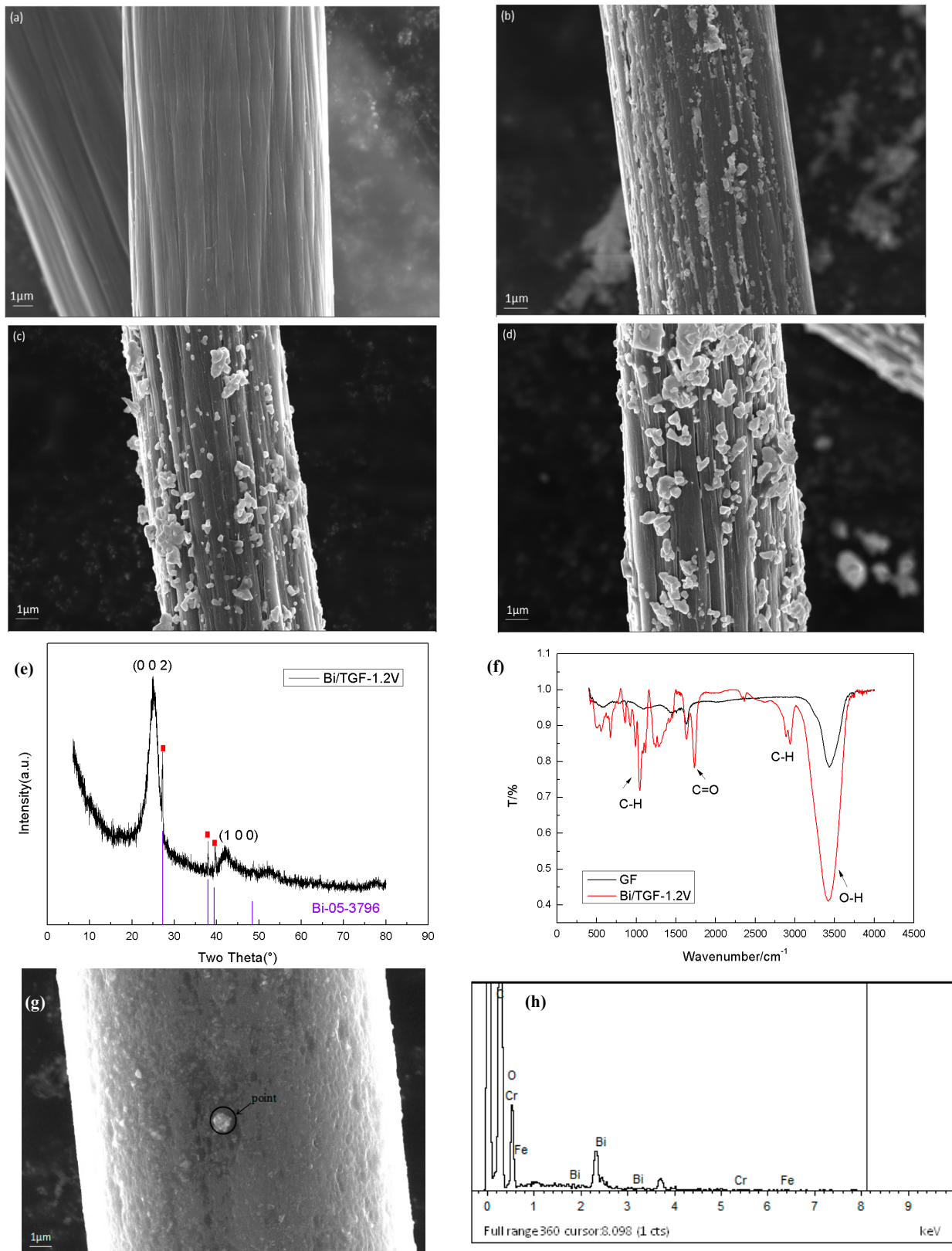


Figure 5. SEM images of TGF and Bi/TGFs: (a) TGF, (b) Bi/TGF-0.8V, (c) Bi/TGF-1.2V, (d) Bi/TGF-1.6V and (e–h) XRD, FTIR and EDX spectrogram (after 20 charge–discharge cycles) of Bi/TGF-1.2V.

3.3. Cell Performance Tests

Figure 6a–c show CE, VE, and EE for VRFB single-cells at current densities from 20 mA/cm² to 80 mA/cm². The CE value of Bi/TGF-1.6V is significantly lower than that of other samples, as reported in Figure 6a. Excessive Bi deposition at 1.6 V increases the consumption of V⁴⁺ ion infiltrated from the positive electrolyte [45], resulting in a significant decrease in CE. Under the same charge–discharge current density, the VE value increases first and then decreases with the increase in electrochemical deposition voltage. As shown in Figure 6b, batteries assembled with Bi/TGF-0.8V and Bi/TGF-1.2V have better charge and discharge efficiency than those with TGF cells. At 80 mA/cm², the VE value of the battery assembled with Bi/TGF-1.2V can reach 86.09%, which is about 8% higher than that of the battery assembled with TGF. However, the electrochemical performance of Bi/TGF-1.6V is worse than that of other felts. This result further confirms the analysis of Bi morphology described above. It can be seen from the SEM results in Figure 5 that the influence of deposition voltage on Bi morphology is significant. The higher the voltage selected, the larger the size of the Bi particles obtained. However, only the battery performance of the sample Bi/TGF-1.2V is good, which indicates that the appropriate Bi particle size can play a role in the battery performance. If the Bi particles are too small in size, then the improvement effect on the battery is not significant. Bi particles with larger sizes are more likely to fall off and may cause a sharp decline in battery performance. At the same time, SEM results of sample Bi/TGF-1.2V also confirmed that after 20 cycles, Bi still remained on the electrode surface, and the battery performance was also improved. In Figure 6c, the trend of EE changes is similar to that of VE, which is attributed to the minor influence of CE. The above results reveal that the electro-deposition of Bi particles on graphite felt can improve the electrochemical performance of vanadium batteries, especially at high current densities. At 80 mA/cm², the efficiency of Bi/TGF-1.6V was significantly reduced. It can be concluded that excessive deposition of Bi particles is not conducive to the electrochemical performance of VRFBs. Figure 6d reports the charge–discharge voltage–capacity of VRFBs using TGF and Bi/TGF electrodes at a current density of 40 mA/cm². Compared with the VRFB assembled with the TGF electrode, the VRFB assembled with the Bi/TGF electrode has a significant decrease in the over-potential during the corresponding charging and discharging process. This is mainly due to the increase in electro-catalytic activity due to the introduction of Bi particles, resulting in a decrease in the charging voltage and an increase in the discharge voltage.

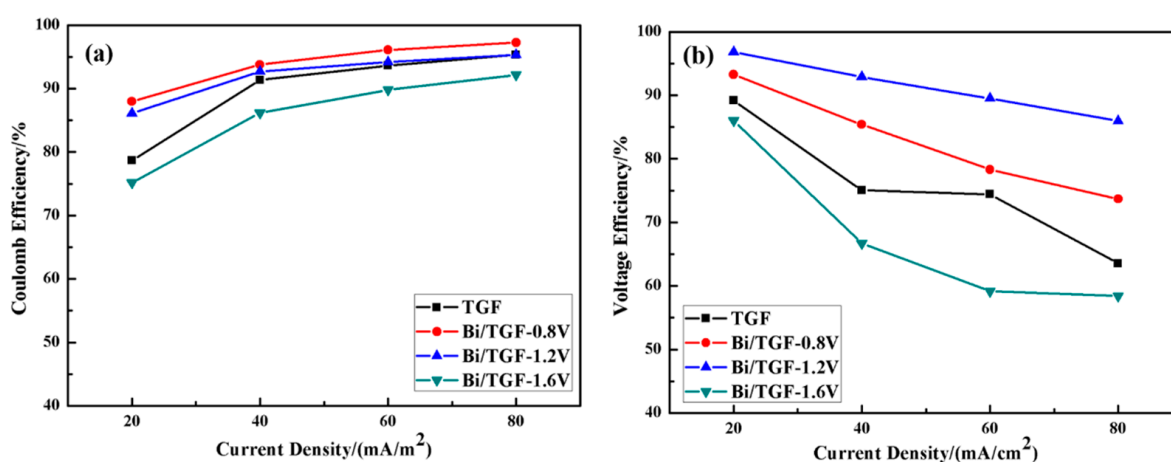


Figure 6. Cont.

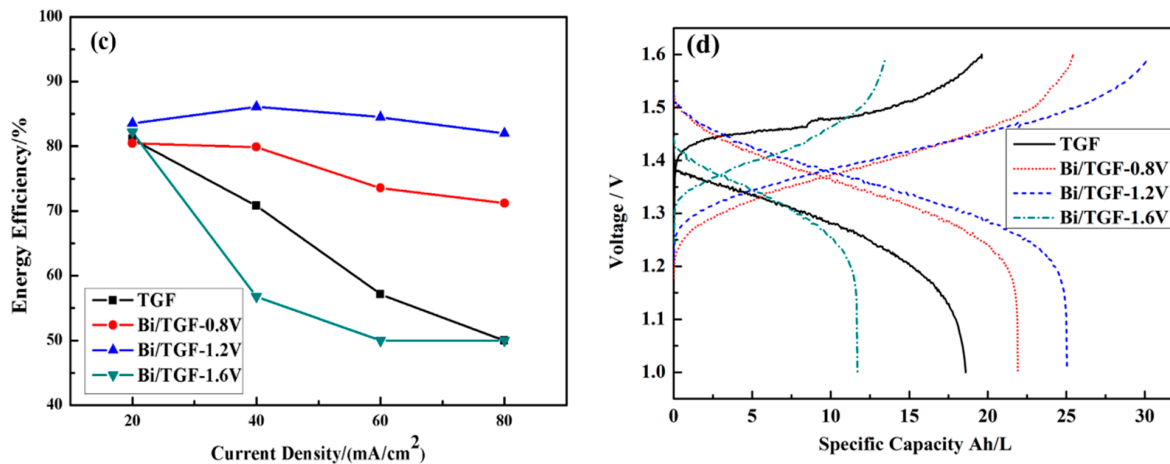


Figure 6. Effects of electrodeposited Bi particles on VRFB: CE (a), VE (b) and EE (c) at constant current densities from 20 mA/cm² to 80 mA/cm², and (d) the voltage profiles of the cells at 40 mA/cm².

To gain further understanding of the effect of Bi catalyst on cell capacity, the changes in charge and discharge capacities of VRFBs at constant current densities from 20 mA/cm² to 80 mA/cm² were investigated (Figure 7). As current density rose, the charge and discharge capacities decreased. The charge capacities of the cell made of Bi/TGF-1.2V electrodes showed the highest values. At the current density of 20 mA/cm², the charge capacities of the cell assembled with Bi/TGF-1.2V electrodes reached 23.348 Ah/L. This value was about 12.62% higher than that for TGF. At the current density of 80 mA/cm², the charge capacities of the cell made of Bi/TGF-1.2V electrodes reached 26.294 Ah/L, while the charge capacities of the cell assembled with TGF declined to yield the lowest value. The increase in capacity was certainly attributed to the effect of Bi particles as the catalyst. However, the efficiency of Bi/TGF-1.6V dropped dramatically at 80 mA/cm². Therefore, excess Bi particles did not benefit the electrochemical performances of VRFBs.

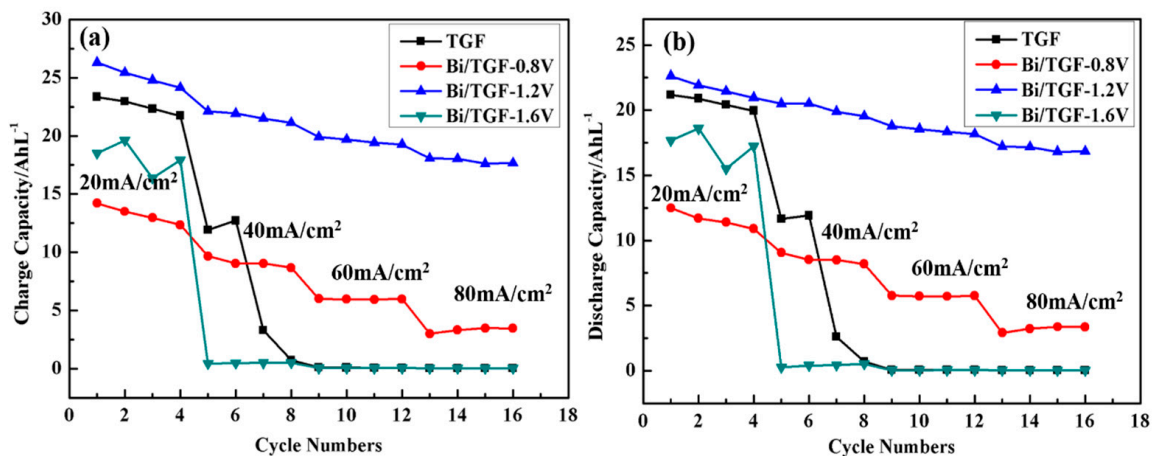


Figure 7. Influence of electrodeposited Bi on VRFB charge capacity (a) and discharge capacity (b) at constant current densities from 20 mA/cm² to 80 mA/cm².

4. Conclusions

The electrochemical deposition of Bi particles can effectively improve the electrochemical performances of redox flow batteries. During the process, Bi was converted to BiH_x during a single battery discharge, promoting the redox reaction of V³⁺/V²⁺. However, excess or less modification will reduce the overvoltage of the redox reaction and aggravate the hydrogen evolution reaction, thus leading to a reduction in battery efficiency. In particular, the optimal Bi-modified electrode was obtained at a deposition voltage of 1.2 V

(Bi/TGF-1.2V). The coulombic efficiency, voltage efficiency and energy efficiency were recorded as 95.50%, 86.14% and 96.81%, respectively. The capacity attenuation rate of the VRFB with Bi/TGF-1.2V decreased significantly at current densities between 20 mA/cm² and 80 mA/cm² when compared to the pristine electrode. Meanwhile, cyclic voltammetry showed the Bi/TGF-1.2V electrode with the highest cathodic peak current, reflecting significant improvements in electrochemical activities towards V³⁺/V²⁺ redox reactions. The electrochemical impedance spectroscopy tests confirmed that the charge transfer resistance of Bi/TGF-1.2V was greatly reduced, which may further improve the electrochemical properties of the VRFB. After 20 cycles, the SEM images indicated that Bi particles were still attached to the surface of graphite fibers, promoting the redox reaction of vanadium ions.

Supplementary Materials: The following supporting information can be downloaded at: <https://www.mdpi.com/article/10.3390/app14083316/s1>, File S1: EDS.

Author Contributions: Conceptualization, H.Z.; methodology, H.Z.; validation, S.C.; formal analysis, S.C. and H.Z.; investigation, S.C. and H.Y.; resources, H.Z.; data curation, W.W.; writing—original draft preparation, S.C., C.S. and H.Z.; writing—review and editing, C.S. and H.Z.; visualization, W.W.; supervision, H.Z.; project administration, S.C. and W.W.; funding acquisition, C.S., H.Z. and W.W. All authors have read and agreed to the published version of the manuscript.

Funding: This work was financially supported by Dalian Polytechnic University in the undergraduate innovation and entrepreneurship training program (Grant No. 202310152007). The authors acknowledge also the 2023 Youth Talent Introduction Scientific Research Startup Fee (Grant No. AUGA2160100623) and 2023 Support Funds for Talent Introduction Units in Heilongjiang Province (Grant No. AUGA2160501723) provided by the Harbin Institute of Technology.

Data Availability Statement: The original contributions presented in the study are included in the article, further inquiries can be directed to the corresponding author.

Conflicts of Interest: The authors declare no conflicts of interest.

References

1. Zhang, H.; Sun, C. Cost-effective iron-based aqueous redox flow batteries for large-scale energy storage application: A review. *J. Power Sources* **2021**, *493*, 229445. [CrossRef]
2. Sun, C.; Zhang, H. Review of the development of first-generation redox flow batteries: Iron-chromium system. *ChemSusChem* **2022**, *15*, e202101798. [CrossRef] [PubMed]
3. Wu, M.; Nan, M.; Ye, Y.; Yang, M.; Qiao, L.; Zhang, H.; Ma, X. A highly active electrolyte for high-capacity iron-chromium flow batteries. *Appl. Energy* **2024**, *358*, 122534. [CrossRef]
4. Perry, M.L.; Saraidaridis, J.D.; Darling, R.M. Crossover mitigation strategies for redox-flow batteries. *Curr. Opin. Electrochem.* **2020**, *21*, 311–318. [CrossRef]
5. Roznyatovskaya, N.; Herr, T.; Küttinger, M.; Fühl, M.; Noack, J.; Pinkwart, K.; Tübke, J. Detection of capacity imbalance in vanadium electrolyte and its electrochemical regeneration for all-vanadium redox-flow batteries. *J. Power Sources* **2016**, *302*, 79–83. [CrossRef]
6. Orapeleng, K.; Wills, R.G.A.; Cruden, A. Developing electrolyte for a soluble lead redox flow battery by reprocessing spent lead acid battery electrodes. *Batteries* **2017**, *3*, 15. [CrossRef]
7. Zeng, Y.; Li, F.; Lu, F.; Zhou, X.; Yuan, Y.; Cao, X.; Xiang, B. A hierarchical interdigitated flow field design for scale-up of high-performance redox flow batteries. *Energy Adv.* **2023**, *2*, 2006–2017. [CrossRef]
8. Lu, W.; Li, X. Advanced membranes boost the industrialization of flow battery. *Acc. Mater. Res.* **2023**, *4*, 681–692. [CrossRef]
9. Jiang, Y.; Liu, Z.; Lv, Y.; Tang, A.; Dai, L.; Wang, L.; He, Z. Perovskite enables high performance vanadium redox flow battery. *Chem. Eng. J.* **2022**, *443*, 136341. [CrossRef]
10. Yu, L.; Lin, F.; Xiao, W.; Xu, L.; Xi, J. Achieving efficient and inexpensive vanadium flow battery by combining Ce_xZr_{1-x}O₂ electrocatalyst and hydrocarbon membrane. *Chem. Eng. J.* **2019**, *356*, 622–631. [CrossRef]
11. Jiang, H.; Sun, J.; Wei, L.; Wu, M.; Shyy, W.; Zhao, T. A high power density and long cycle life vanadium redox flow battery. *Energy Storage Mater.* **2020**, *24*, 529–540. [CrossRef]
12. Jang, J.; Shin, M.; Kwon, Y.; Jo, C. Carbon cloth modified by direct growth of nitrogen-doped carbon nanofibers and its utilization as electrode for zero gap flow batteries. *Chem. Eng. J.* **2024**, *481*, 148644. [CrossRef]
13. Zhang, H.; Chen, N.; Sun, C.; Luo, X. Investigations on physicochemical properties and electrochemical performance of graphite felt and carbon felt for iron-chromium redox flow battery. *Int. J. Energy Res.* **2020**, *44*, 3839–3853. [CrossRef]

14. Sun, C.; Negro, E.; Nale, A.; Pagot, G.; Vezzù, K.; Zawodzinski, T.A.; Meda, L.; Gambaro, C.; Di Noto, V. An efficient barrier toward vanadium crossover in redox flow batteries: The bilayer [Nafion/(WO₃)_x] hybrid inorganic-organic membrane. *Electrochim. Acta* **2021**, *378*, 138133. [[CrossRef](#)]
15. Shanahan, B.; Seteiz, K.; Heizmann, P.A.; Koch, S.; Büttner, J.; Ouardi, S.; Vierrath, S.; Fischer, A.; Breitwieser, M. Rapid wet-chemical oxidative activation of graphite felt electrodes for vanadium redox flow batteries. *RSC Adv.* **2021**, *11*, 32095–32105. [[CrossRef](#)] [[PubMed](#)]
16. Mazur, P.; Mrlik, J.; Pocedic, J.; Vrana, J.; Dundalek, J.; Kosek, J.; Bystron, T. Effect of graphite felt properties on the long-term durability of negative electrode in vanadium redox flow battery. *J. Power Sources* **2019**, *414*, 354–365. [[CrossRef](#)]
17. Deng, Q.; HuangYang, X.; Zhang, X.; Xiao, Z.; Zhou, W.; Wang, H.; Liu, H.; Zhang, F.; Li, C.; Wu, X.; et al. Edge-rich multidimensional frame carbon as high-performance electrode material for vanadium redox flow batteries. *Adv. Energy Mater.* **2022**, *12*, 2103186. [[CrossRef](#)]
18. Ghimire, P.C.; Schweiss, R.; Scherer, G.G.; Lim, T.M.; Wai, N.; Bhattarai, A.; Yan, Q. Optimization of thermal oxidation of electrodes for the performance enhancement in all-vanadium redox flow battery. *Carbon* **2019**, *155*, 176–185. [[CrossRef](#)]
19. Hyun, K.; Shin, M.; Kwon, Y. Performance evaluation of zero-gap vanadium redox flow battery using composite electrode consisting of graphite and buckypaper. *Korean J. Chem. Eng.* **2022**, *39*, 3315–3322. [[CrossRef](#)]
20. Sun, B.; Skyllas-Kazacos, M. Modification of graphite electrode materials for vanadium redox flow battery application—Part I. Thermal treatment. *Electrochim. Acta* **1992**, *37*, 1253–1260. [[CrossRef](#)]
21. Sun, B.; Skyllas-Kazacos, M. Chemical modification of graphite electrode materials for vanadium redox flow battery application—Part II. Acid treatments. *Electrochim. Acta* **1992**, *37*, 2459–2465. [[CrossRef](#)]
22. Yoon, S.J.; Kim, S.; Kim, D.K.; So, S.; Hong, Y.T.; Hempelmann, R. Ionic liquid derived nitrogen-doped graphite felt electrodes for vanadium redox flow batteries. *Carbon* **2020**, *166*, 131–137. [[CrossRef](#)]
23. Park, S.E.; Yang, S.Y.; Kim, K.J. Boron-functionalized carbon felt electrode for enhancing the electrochemical performance of vanadium redox flow batteries. *Appl. Surf. Sci.* **2021**, *546*, 148941. [[CrossRef](#)]
24. Yang, I.; Lee, S.; Jang, D.; Lee, J.-E.; Cho, S.Y.; Lee, S. Enhancing energy efficiency and long-term durability of vanadium redox flow battery with catalytically graphitized carbon fiber felts as electrodes by boron doping. *Electrochim. Acta* **2022**, *429*, 141033. [[CrossRef](#)]
25. Gautam, R.K.; Kapoor, M.; Verma, A. Tactical surface modification of a 3D graphite felt as an electrode of vanadium redox flow batteries with enhanced electrolyte utilization and fast reaction kinetics. *Energy Fuels* **2020**, *34*, 5060–5071. [[CrossRef](#)]
26. Kaur, A.; Jeong, K.I.; Kim, S.S.; Lim, J.W. Optimization of thermal treatment of carbon felt electrode based on the mechanical properties for high-efficiency vanadium redox flow batteries. *Compos. Struct.* **2022**, *290*, 115546. [[CrossRef](#)]
27. Kim, J.; Park, H. Recent advances in porous electrodes for vanadium redox flow batteries in grid-scale energy storage systems: A mass transfer perspective. *J. Power Sources* **2022**, *545*, 231904. [[CrossRef](#)]
28. Wang, S.; Xu, Z.; Wu, X.; Zhao, H.; Zhao, J.; Liu, J.; Yan, C.; Fan, X. Excellent stability and electrochemical performance of the electrolyte with indium ion for iron–chromium flow battery. *Electrochim. Acta* **2020**, *368*, 137524. [[CrossRef](#)]
29. Zhang, X.Y.; Valencia, A.; Li, W.L. Decoupling activation and transport by electron-regulated atomic-Bi harnessed surface-to-pore interface for vanadium redox flow battery. *Adv. Mater.* **2023**, *36*, 2305415. [[CrossRef](#)]
30. Xie, C.; Yan, H.; Song, Y.; Song, Y.; Yan, C.; Tang, A. Catalyzing anode Cr²⁺/Cr³⁺ redox chemistry with bimetallic electrocatalyst for high-performance iron-chromium flow batteries. *J. Power Sources* **2023**, *564*, 232860. [[CrossRef](#)]
31. Chen, F.; Cheng, X.; Liu, L.; Han, L.; Liu, J.; Chen, H.; Zhang, Q.; Yan, C. Modification of carbon felt electrode by MnO@C from metal-organic framework for vanadium flow battery. *J. Power Sources* **2023**, *580*, 233421. [[CrossRef](#)]
32. Xiang, Y.; Daoud, W.A. Investigation of an advanced catalytic effect of cobalt oxide modification on graphite felt as the positive electrode of the vanadium redox flow battery. *J. Power Sources* **2019**, *416*, 175–183. [[CrossRef](#)]
33. Kabtamu, D.M.; Bayeh, A.W.; Chiang, T.C.; Chang, Y.C.; Lin, G.Y.; Wondimu, T.H.; Su, S.K.; Wang, C.H. TiNb₂O₇ nanoparticle-decorated graphite felt as a high-performance electrode for vanadium redox flow batteries. *Appl. Surf. Sci.* **2018**, *462*, 73–80. [[CrossRef](#)]
34. Yang, H.; Fan, C.; Zhu, Q. Sucrose pyrolysis assembling carbon nanotubes on graphite felt using for vanadium redox flow battery positive electrode. *J. Energy Chem.* **2018**, *27*, 451–454. [[CrossRef](#)]
35. Fu, H.; Bao, X.; He, M.; Xu, J.; Miao, Z.; Ding, M.; Liu, J.; Jia, C. Defect-rich graphene skin modified carbon felt as a highly enhanced electrode for vanadium redox flow batteries. *J. Power Sources* **2022**, *556*, 232443. [[CrossRef](#)]
36. Opar, D.O.; Nankya, R.; Lee, J.; Jung, H. Three-dimensional mesoporous graphene-modified carbon felt for high-performance vanadium redox flow batteries. *Electrochim. Acta* **2020**, *330*, 135276. [[CrossRef](#)]
37. Li, B.; Gu, M.; Nie, Z.; Shao, Y.; Luo, Q.; Wei, X.; Li, X.; Xiao, J.; Wang, C.; Sprenkle, V.; et al. Bismuth nanoparticle decorating graphite felt as a high-performance electrode for an all-vanadium redox flow battery. *Nano Lett.* **2013**, *13*, 1330–1335. [[CrossRef](#)] [[PubMed](#)]
38. Suárez, D.J.; González, Z.; Blanco, C.; Granda, M.; Menéndez, R.; Santamaría, R. Graphite felt modified with bismuth nanoparticles as negative electrode in a vanadium redox flow battery. *ChemSusChem* **2014**, *7*, 914–918. [[CrossRef](#)] [[PubMed](#)]
39. Flox, C.; Murcia-López, S.; Carretero, N.M.; Ros, C.; Morante, J.R.; Andreu, T. Role of bismuth in the electrokinetics of silicon photocathodes for solar rechargeable vanadium redox flow batteries. *ChemSusChem* **2018**, *11*, 125–129. [[CrossRef](#)]

40. Yang, X.; Liu, T.; Xu, C.; Zhang, H.; Li, X.; Zhang, H. The catalytic effect of bismuth for $\text{VO}^{2+}/\text{VO}^{2+}$ and $\text{V}^{3+}/\text{V}^{2+}$ redox couples in vanadium flow batteries. *J. Energy Chem.* **2017**, *26*, 1–7. [[CrossRef](#)]
41. Yang, Z.; Wei, Y.; Zeng, Y.; Yuan, Y. Effects of in-situ bismuth catalyst electrodeposition on performance of vanadium redox flow batteries. *J. Power Sources* **2021**, *506*, 230238. [[CrossRef](#)]
42. Che, H.X.; Gao, Y.F.; Yang, J.H.; Hong, S.; Hao, L.D.; Xu, L.; Taimoor, S.; Robertson, A.W.; Sun, Z.Y. Bismuth nanoparticles anchored on N-doped graphite felts to give stable and efficient iron-chromium redox flow batteries. *New Carbon Mater.* **2024**, *39*, 131–141. [[CrossRef](#)]
43. Zhang, Q.A.; Yan, H.; Song, Y.; Yang, J.; Song, Y.; Tang, A. Boosting anode kinetics in vanadium flow batteries with catalytic bismuth nanoparticle decorated carbon felt *via* electro-deoxidization processing. *J. Mater. Chem. A* **2023**, *11*, 8700–8709. [[CrossRef](#)]
44. Zhou, X.; Zhang, X.; Mo, L.; Zhou, X.; Wu, Q. Densely populated bismuth nanosphere semi-embedded carbon felt for ultrahigh-rate and stable vanadium redox flow batteries. *Small* **2020**, *16*, e1907333. [[CrossRef](#)] [[PubMed](#)]
45. Ren, J.; Wang, Z.; Sun, J.; Guo, Z.; Liu, B.; Fan, X.; Zhao, T. In-situ electrodeposition of homogeneous and dense bismuth nanoparticles onto scale-up graphite felt anodes for vanadium redox flow batteries. *J. Power Sources* **2023**, *586*, 233655. [[CrossRef](#)]
46. Eifert, L.; Jusys, Z.; Behm, R.; Zeis, R. Side reactions and stability of pre-treated carbon felt electrodes for vanadium redox flow batteries: A DEMS study. *Carbon* **2020**, *158*, 580–587. [[CrossRef](#)]
47. Sun, C.; Negro, E.; Vezzù, K.; Pagot, G.; Cavinato, G.; Nale, A.; Bang, Y.H.; Di Noto, V. Hybrid inorganic-organic proton-conducting membranes based on SPEEK doped with WO_3 nanoparticles for application in vanadium redox flow batteries. *Electrochim. Acta* **2019**, *309*, 311–325. [[CrossRef](#)]
48. Kim, K.J.; Park, M.-S.S.; Kim, Y.-J.J.; Kim, J.H.; Dou, S.X.; Skyllas-Kazacos, M. A technology review of electrodes and reaction mechanisms in vanadium redox flow batteries. *J. Mater. Chem. A* **2015**, *3*, 16913–16933. [[CrossRef](#)]
49. Noack, J.; Berkers, M.; Ortner, J.; Pinkwart, K. The Influence of some electrolyte additives on the electrochemical performance of Fe/Fe^{2+} redox reactions for iron/iron redox flow batteries. *J. Electrochem. Soc.* **2021**, *168*, 040529. [[CrossRef](#)]
50. Solhy, A.; Machado, B.; Beausoleil, J.; Kihn, Y.; Gonçalves, F.; Pereira, M.; Órfão, J.; Figueiredo, J.; Faria, J.; Serp, P. MWCNT activation and its influence on the catalytic performance of Pt/MWCNT catalysts for selective hydrogenation. *Carbon* **2008**, *46*, 1194–1207. [[CrossRef](#)]

Disclaimer/Publisher’s Note: The statements, opinions and data contained in all publications are solely those of the individual author(s) and contributor(s) and not of MDPI and/or the editor(s). MDPI and/or the editor(s) disclaim responsibility for any injury to people or property resulting from any ideas, methods, instructions or products referred to in the content.